

SLIP-RUNNING RECONNECTION IN QUASI-SEPARATRIX LAYERS

G. AULANIER, E. PARIAT*, and P. DÉMOULIN

*Observatoire de Paris, Laboratoire d'Etudes Spatiales et d'Instrumentation en Astrophysique,
F-92195 Meudon Cedex, France*

and

C.R. DEVORE

*Naval Research Laboratory, Laboratory for Computational Physics and Fluid Dynamics,
Washington, DC 20375, USA*

(Received 31 May 2006; accepted 19 September 2006; Published online 8 November 2006)

Abstract. Using time dependent MHD simulations, we study the nature of three-dimensional magnetic reconnection in thin quasi-separatrix layers (QSLs), in the absence of null points. This process is believed to take place in the solar atmosphere, in many solar flares and possibly in coronal heating. We consider magnetic field configurations which have previously been weakly stressed by asymmetric line-tied twisting motions and whose potential fields already possessed thin QSLs. When the line-tied driving is suppressed, magnetic reconnection is solely due to the self-pinching and dissipation of narrow current layers previously formed along the QSLs. A generic property of this reconnection process is the continuous slippage of magnetic field lines along each other, while they pass through the current layers. This is contrary to standard null point reconnection, in which field lines clearly reconnect by pair and abruptly exchange their connectivities. For sufficiently thin QSLs and high resistivities, the field line footpoints slip-run at super-Alfvénic speeds along the intersection of the QSLs with the line-tied boundary, even though the plasma velocity and resistivity are there fixed to zero. The slip-running velocities of a given footpoint have a well-defined maximum when the field line crosses the thinnest regions of the QSLs. QSLs can then physically behave as true separatrices on MHD time scales, since magnetic field lines can change their connections on time scales far shorter than the travel-time of Alfvén waves along them. Since particles accelerated in the diffusive regions travel along the field much faster than the Alfvén speed, slip-running reconnection may also naturally account for the fast motion of hard X-ray sources along chromospheric ribbons, as observed during solar flares.

1. Introduction

Due to its low plasma β , the solar corona is a medium which is governed by magnetic fields. The energy which is needed to power intense flares and to sustain quasi-steady coronal heating is there stored in non-potential magnetic fields. In plasmas with a high Reynolds number, MHD theory states that magnetic energy can only be released in localized regions where magnetic fields have small-scale gradients, i.e. in narrow current layers. The diffusion of magnetic fields in such current layers naturally leads to magnetic reconnection (Sweet, 1958). During confined and

*Université Paris 7–Denis Diderot, 75251 Paris Cedex 05, France.

eruptive solar flares, this process is believed to occur in magnetic configurations that have a complex topology (see the reviews of Longcope, 2005; Démoulin, 2006). The same physics is also invoked to model coronal heating when the photospheric distribution of flux shows multiple concentrations (*e.g.* Démoulin and Priest, 1997; Wang *et al.*, 2000; Fletcher *et al.*, 2001; Priest, Heyvaerts, and Title, 2002; Priest, Longcope, and Heyvaerts, 2005).

Complex topologies can be separated into two classes: first, the ones defined by separatrix surfaces and second, the ones defined by quasi-separatrix layers. Separatrices are formed by the ensemble of magnetic field lines which pass either through a null point (NP, see Lau, 1993) or through a bald patch (BP, see Titov, Priest, and Démoulin, 1993), and the connectivity of magnetic field lines is discontinuous across them. In this case, separators are singular field lines defined by the intersection of two separatrices. Quasi-separatrix layers (QSLs) are narrow volumes across which the magnetic field connectivity remains continuous, though it has strong variations (Priest and Démoulin, 1995; Démoulin, Priest, and Lonie, 1996; Démoulin *et al.*, 1996). In a bounded physical domain, this occurs for example when the domain boundaries are placed so as to exclude all NPs from the domain interior and BPs from its boundary (see Démoulin *et al.*, 1996). A QSL is a purely three-dimensional object. In a given QSL, the connectivity gradients are the largest in the sub-region where the squashing degree Q (defined by Titov, Hornig, and Démoulin, 2002) peaks to its maximum value, which is known as the hyperbolic flux tube (HFT, see Titov, Gaslaard, and Neukirch, 2003). In 3D magnetic configurations defined by several flux concentrations, QSLs (and HFTs) become separatrices (and separators) as their width (*resp.* squashing degree) asymptotically tend to zero (*resp.* infinity).

In the case of NP separatrices, the spontaneous formation of current sheets for any line-tied motion has been shown analytically (Low and Wolfson, 1988; Aly, 1990; Lau, 1993) and numerically (*e.g.* Yokoyama and Shibata, 1994; Ma *et al.*, 1995; Karpen *et al.*, 1998, Longcope and Magara, 2004). The same conclusions were obtained for BP separatrices (*e.g.* Low and Wolfson, 1988; Billinghurst, Craig, and Sneyd, 1993), but they are still debated because of the issue of the efficiency of line-tying in BPs (Karpen, Antiochos, and DeVore, 1991; Delannée and Aulanier, 1999).

There have been numerous studies about magnetic reconnection occurring in separatrices. One of the main objectives, especially in local 2D and 2.5D (invariant by translation) NP configurations, has been the finding of fast reconnection regimes, either in the frame of resistive MHD (see *e.g.* Petschek, 1964; Strauss, 1986; Priest and Forbes, 1992a; Craig and McClymont, 1993; Baty, Priest, and Forbes, 2006) or of Hall MHD, which supports reconnection through collisionless processes (see *e.g.* Ma and Bhattacharjee, 2001; Bhattacharjee, Ma, and Wang, 2003). Another objective has been the identification of all existing classes of reconnections in local 3D NP configurations (as reviewed in Priest and Forbes, 2000). Global models involving the NP and the surrounding arcades, taking into account the geometry

and the line-tied boundary conditions, have been calculated so as to mimic solar observed phenomena (*e.g.* Yokoyama and Shibata, 1994; Karpen *et al.*, 1998). One natural result of these models is that NP reconnection involves two field lines at a time, whose footpoints exchange their connectivity abruptly when they reconnect, whatever the reconnection rate. This is a natural consequence of the discontinuous connectivity across separatrices.

The case of QSLs (and HFTs) has been more difficult to address, mostly because of mathematical and conceptual difficulties. Démoulin *et al.* (1996) first proposed some analytical arguments in favor of current sheet formation in narrow QSLs already existing in any magnetic configuration (even in a potential field) whatever the footpoint motions are. This conjecture was strongly debated by the analytical calculations of Inverarity and Titov (1997) and by the numerical experiments of Galsgaard (2000) and Galsgaard, Titov, and Neukirch (2003). They all argued that specific footpoint motions are required to generate intense current layers in a QSL, through the pinching of its HFT. This approach was also used by de Moortel and Galsgaard (2006) to set MHD calculations of current sheet formation in pre-existing separatrices and dynamically formed QSLs. In Aulanier, Pariat, and Démoulin (2005, hereafter Paper I), we performed new numerical experiments to address this issue. We modeled more realistic solar magnetic configurations (*i.e.* with one single line-tied plane, closed magnetic field lines and magnetic field decreasing away from well-defined flux concentrations). We partly explored the parameter space, both for the magnetic models and for the prescribed footpoint motions. We found that, as conjectured by Démoulin *et al.* (1996), narrow current layers spontaneously develop all along the QSLs, for any smooth and large-scale footpoint motion. We also found that the strongest currents always develop in the vicinity of the HFT, though their detailed shape and magnitude still depend on the boundary driving. In a completely independent but similar study, Büchner (2005, 2006) also calculated the natural formation of current sheets along QSLs, in an MHD model of an observed X-ray bright point starting from a magnetic field extrapolation of an observed magnetogram.

Following Paper I, thus considering that current sheets do naturally form along QSLs in a similar way as they do in separatrices, a question which then arises is, what is the nature of magnetic reconnection in QSLs (and HFTs)? This is the topic of the present paper.

The question of separatrix-less reconnection was first addressed by Hesse and Schindler (1988). They demonstrated that the existence of parallel electric and magnetic fields was the condition for general 3D reconnection. To the authors' knowledge, Priest and Forbes (1992b) were the first to envision that, when reconnection occurs without true separatrices in 3D, magnetic field lines must slip along each other within so-called magnetic flipping layers. These layers are the remnants of 2D X-shaped separatrices in 2.5D configuration invariant by translation. Priest and Démoulin (1995) further developed this concept in 3D, by introducing the QSLs. Under the assumption that field lines simply exchange their connectivity

with that of their neighbors, as one of their footpoints is displaced in time across a QSL, they proposed that magnetic flipping occurs in a QSL when the sub-Alfvénic displacement of one field line footpoint across the QSL results in a super-Alfvénic displacement of the other footpoint. Such mechanism, though, is hardly justified in the frame of MHD. So, using the straight and thick HFT configuration developed by Titov, Galsgaard, and Neukirch (2003), having a clear X-type configuration in an extended region located between two facing line-tied plates, Priest, Hornig, and Pontin (2003) developed a kinematic model of 3D reconnection, driven by long-duration, continuous and symmetric footpoint motions. They showed that the prescribed driving must lead to field line slippage when the HFT gets sufficiently pinched.

Using space and time varying resistivities and following the simulations of Galsgaard, Titov, and Neukirch (2003), full MHD experiments of this kinematic model were performed by Pontin *et al.* (2005). These 3D simulations were consistent with earlier findings (Hesse and Schindler, 1988; Priest and Forbes, 1992b; Priest, Hornig, and Pontin, 2003) and they further showed that the reconnection jets emanating from the diffusion region had little relation with the velocities of the slipping field lines. Field line slippage was also recently reported in MHD simulations of prominence merging in 3D (DeVore, Antiochos, and Aulanier, 2005; Aulanier, DeVore, and Antiochos, 2006). There, magnetic reconnection was driven by the progressive shearing of two initially potential dipoles located next to each other along a shared inversion line.

There are still questions unaddressed by the simulations of Pontin *et al.* (2005) and DeVore, Antiochos, and Aulanier (2005), regarding the nature of 3D magnetic reconnection in narrow QSLs. Firstly, the studied magnetic field configurations had very broad initial HFTs: the initial squashing degree was $Q \sim 40$ in Pontin *et al.* (2005) and $Q \sim 2$ in DeVore, Antiochos, and Aulanier (2005), respectively. We argue that the reconnecting current layers in these calculations were therefore not due to any initial complex topology. They are probably rather due to the progressive development of shear layers thanks to the boundary driving, very much like in flux braiding experiments (see *e.g.* Longbottom *et al.*, 1998). Secondly, (nearly) continuous and relatively fast line-tied driving velocities were applied in both calculations. They were of the order of 10% of the Alfvén speed around the reconnecting layers within the domain. Such drivings preclude the precise derivation of slippage velocities when they are sub-Alfvénic, since field line footpoints are also evolved by the line-tied motions. So the relation between the topology (i.e. the thickness of pre-existing QSLs) and the slippage velocities of reconnecting field lines could not be, and therefore was not addressed in these experiments.

In this paper, we explicitly study this issue. We find in particular that for sufficiently thin QSLs and for high enough resistivities, field line footpoints can shift super-Alfvénically along the arc-shaped intersection of the QSLs with the line-tied plane. The speed of this process leads us to call it *slip-running reconnection*, in

opposition to mild and slow diffusive slippage. The absence of artificial symmetries in our models also permits us to reveal reconnections in opposite senses at the same time in different locations in the QSLs, and allows us to derive observational consequences for the evolution of EUV and hard X-ray emission along flare ribbons.

2. Numerical Experiments

2.1. PREVIOUSLY STRESSED MAGNETIC CONFIGURATIONS

In Paper I, we considered two magnetic field configurations. Even though they were strictly speaking bipolar, they were formed by two bipolar flux concentrations, with non-zero magnetic flux away from the center of the four main polarity concentrations. Both configurations were labeled by the angle Φ made by the inner and the outer bipole (i.e. $\Phi = 150^\circ$ and 120°). The size of the inner bipole was $L = 0.2$, and the size of the outer bipole was 1. The maximum vertical field in the inner bipole was $b_o = 35$. The magnetic energies of the associated potential field were $E_b^0 = 5.99$ and 6.96 for $\Phi = 150^\circ$ and 120° , respectively. Both corresponding potential fields possessed very thin QSLs and a HFT, though their thicknesses were much smaller for $\Phi = 150^\circ$ than for 120° . The maximum squashing degrees in the center of the HFT for the potential fields were $Q = 6 \times 10^8$ and $Q = 4 \times 10^4$ for $\Phi = 150^\circ$ and 120° , respectively.

We performed zero- β resistive MHD simulations of the development of electric currents in both initially potential configurations. To do so, we applied smooth and extended line-tied sub-Alfvénic translational and twisting motions, of one polarity of the inner bipole only. Thus, the prescribed motions and the evolving magnetic fields were asymmetric. In this paper, we analyze magnetic reconnection in the configurations evolved by the twisting motions only.

Since the initial Alfvén speed was homogeneous, being $c_A = 0.2$ in our non-dimensionalized units, the time unit t_A was then defined as the travel-time of Alfvén waves from one magnetic polarity to the other in the inner bipole. The plasma resistivity was low and uniform: $\eta = 1.5 \times 10^{-6}$. This value will further be referred to as η^* throughout the paper.

While narrow electric layers always spontaneously developed within the QSLs, the strongest of these currents developed in the vicinity of the HFTs. There, the current layers progressively got thinner during the driven evolution, until they eventually reached the scale of the mesh at $t = t^\circ$, thus halting the calculations. Using the twisting motions, we reached $t^\circ = 39.2 t_A$ (resp. $102.5 t_A$) for $\Phi = 150^\circ$ (resp. 120°). These different times were due to the differences in QSL thickness. We showed that more free magnetic energy could be injected in configurations having broader QSLs, before the currents reached the dissipative scale.

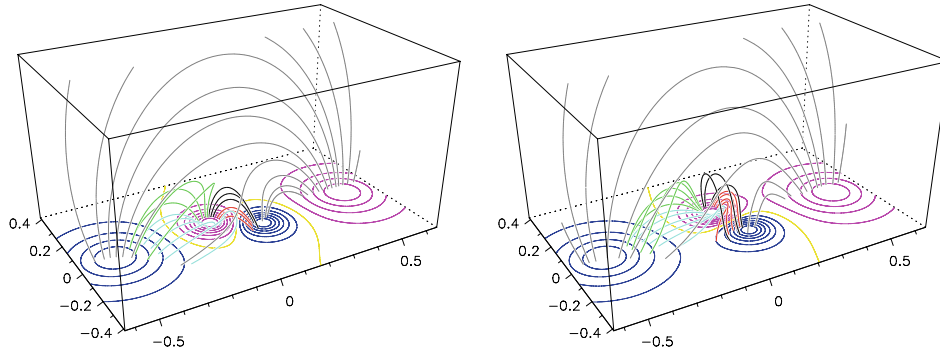


Figure 1. Projection views of the two stressed magnetic field configurations, labeled $\Phi = 150^\circ$ (left panel) and $\Phi = 120^\circ$ (right panel), used as initial conditions for resistive relaxations. The (pink; blue) contours at $z = 0$ stand for (positive; negative) values of $b_z(z = 0)$ and the yellow line shows the inversion line $b_z(z = 0) = 0$. The colored lines are magnetic field lines. The configuration $\Phi = 150^\circ$ (resp. 120°) was previously evolved from its potential field at $t = 0$, up to $t = t^* = 34$ (resp. $t^* = 90$), using sub-Alfvénic twisting motions within the positive polarity of the inner bipole. The whole numerical domain is shown.

2.2. MHD RELAXATIONS

In this paper, we consider as initial magnetic fields the configurations shown in Figure 1. Each of them correspond to one Φ value, and both have previously been evolved by twisting motions as described above, up to the time $t^* = 34 t_A$ (resp. $90 t_A$) for $\Phi = 150^\circ$ (resp. 120°). These times were chosen to ensure that the current layers were sufficiently developed in the QSLs, while they still remained resolved over several mesh points, and so as to consider two comparable models, having approximately the same thicknesses for the current layer in their HFT. Their free magnetic energy δE_b , defined as the excess to the potential field energy, is $\delta E_b/E_b^0 = 0.25\%$ (resp. 2%) for $\Phi = 150^\circ$ (resp. 120°).

We perform numerical calculations in cartesian geometry of zero- β resistive MHD relaxations of both initial stressed magnetic field configurations. The x axis is parallel to the orientation of the outer bipole and the z axis is the altitude. The two following equations are used for the time integration, from $t = t^*$:

$$\frac{\partial \mathbf{u}}{\partial t} = -(\mathbf{u} \cdot \nabla) \mathbf{u} + \rho^{-1} \mathbf{j} \times \mathbf{b} + D_{\mathbf{u}}, \quad (1)$$

$$\frac{\partial \mathbf{b}}{\partial t} = \nabla \times (\mathbf{u} \times \mathbf{b}) + \eta \Delta \mathbf{b}, \quad (2)$$

ρ being the mass density, \mathbf{u} the plasma velocity, \mathbf{b} the magnetic field, \mathbf{j} the electric current density and η the magnetic resistivity. Equations (1) and (2) are solved using:

$$\rho(t) = \rho(t = 0) = 25 b^2(t = 0) \quad (3)$$

$$\nabla \times \mathbf{b} = \mathbf{j}, \quad (4)$$

$$\nabla \cdot \mathbf{b} = 0. \quad (5)$$

We use line-tied conditions at $z = 0$ to simulate the solar photosphere and open conditions at the five other domain boundaries. Three relaxations are performed for each configuration, using three values for the uniform resistivities $\eta = \eta^*, 3\eta^*$ and $10\eta^*$. At the scale of L , the corresponding Lundquist numbers are $Lu \sim 27000, 9000$ and 2700 . At $t = t^*$, all velocities are reset to zero. During these relaxations, the resistivity and the velocities at the line-tied boundary are $\eta = 0$ and $\mathbf{u}(z = 0) = \mathbf{0}$.

Apart from the resistive parameter and the suppression of the boundary driving, the relaxations are calculated with the same exact conditions as in the continuously driven calculations reported in Paper I. The viscous filter $D_{\mathbf{u}}$ is adapted to the local cell size in the domain. It is set up to give a minimum characteristic viscous speed of $0.15 c_A$. This amplitude is required to ensure numerical stability in the HFT for the high- Lu regimes considered in the relaxations. The calculations are performed with $n_x \times n_y \times n_z = 191 \times 161 \times 170$ mesh points, distributed non uniformly in the domain. The smallest cell has a size of $d = 1.5 \times 10^{-3}$ and is located at the center of the inner bipole at $z = 0$.

Non-zero velocities naturally develop in the domain. The origin and effects of the residual Lorentz forces which generate these velocities are respectively discussed in Section 3 and in Section 4.

3. Magnetic Reconnection Trigger

3.1. CO-EXISTENCE OF TWO CURRENT LAYERS IN THE QSLs

At $t = t^*$, the QSLs are slightly deformed from their original shape (when the field was potential). Narrow current layers are present all along the 3D thin volume defined by the QSLs (see Paper I). More specifically, two well developed narrow current layers appear within the QSLs, where their 3D deformations are the strongest. Figure 2 shows these layers for $\Phi = 150^\circ$, at $t = t^* + 2$ in the early stages of a relaxation. In its middle row, the signed quantity α is plotted, being defined as:

$$\alpha = \mathbf{j} \cdot \mathbf{b}/b^2. \quad (6)$$

It has the dimension of the inverse of a length. It indicates both the sign of $\mathbf{j} \cdot \mathbf{b}$ and the scale-length of the magnetic field gradients, i.e. the approximate thickness of the current layers at FWHM. This quantity thus permits to focus on the QSL-related narrow current sheets. It minimizes the visibility of strong, but extended and therefore less diffusive, force-free volume currents. For $y > 0$ one current layer is roughly horizontal (i.e. orthogonal to the z axis), while for $y < 0$ another layer is roughly vertical (i.e. parallel to the z axis). Figure 2 shows that the horizontal current

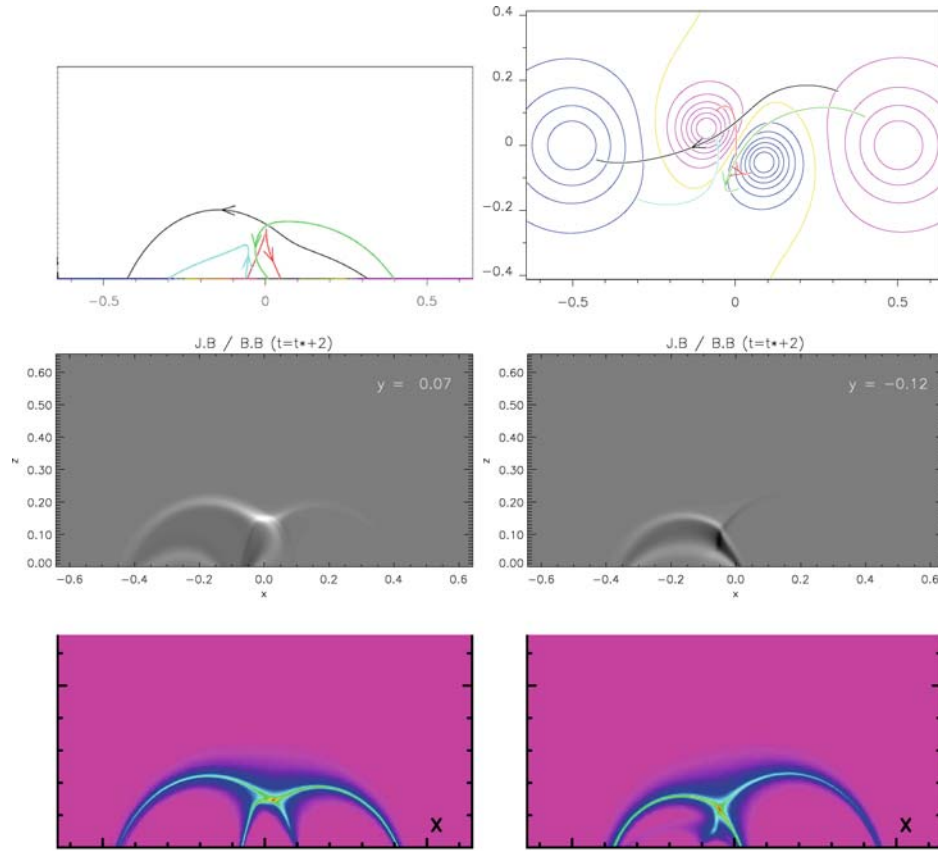


Figure 2. Magnetic field lines, electric currents and QSLs during the resistive relaxation of the configuration $\Phi = 150^\circ$, at $t = t^* + 2$, using $\eta = 15 \times 10^{-6}$. *Top row:* 3D projection views of four magnetic field lines, passing in the vicinity of the two narrowest current layers that are present in the QSLs at $y = 0.07$ and $y = -0.12$. Two projections are shown, along the y axis (*left panel*) and along the z axis, i.e. as viewed from above (*right panel*). The contours of $b_z(z = 0)$ are the same as in Figure 1. *Middle row:* 2D maps of $\alpha = \mathbf{j} \cdot \mathbf{b} / b^2$, drawn at $y = 0.07$ (*left panel*) and at $y = -0.12$ (*right panel*). The color coding is saturated, so that (black; white) stand for $\alpha = (-36; 36)$. *Bottom row:* 2D maps of the squashing degree Q in the QSLs in the same $y = \text{constant}$ planes. The (red ; yellow; green; cyan; blue; pink) colors stand for $Q = (10^8; 3 \cdot 10^6; 10^5; 5 \cdot 10^3; 50; 2)$. The central part of the HFT is thus drawn in red.

layer has $\alpha > 0$ whereas the vertical current layer has $\alpha < 0$. Analogous currents are present for $\Phi = 120^\circ$, but there the vertical current layer is less pronounced.

This system of so-called “direct” and “return” currents finds its origin in the early slow and confined counter-clockwise twisting of the initially potential fields. The azimuthal velocity profile in the vortex had a sine-like profile (see Paper I for its exact expression). The direct currents are there approximately located in the ensemble of field lines which are rooted in the area where the previous twisting

velocities increased away from the vortex center, i.e. in the inner part of the vortex. Oppositely, the return currents are located in the outer part of the vortex, where the twisting velocities decreased toward the external untwisted regions. In the region of direct currents, the electric current J_{\parallel} projected onto the magnetic field \mathbf{b} is antiparallel to the magnetic field, so that $\alpha < 0$. In the region of return currents, J_{\parallel} is parallel to \mathbf{b} , so that $\alpha > 0$. It follows that the horizontal current layer is located in the region of return currents, whereas the vertical current layer is located in the region of direct currents.

Vertical cuts of the squashing degree Q , which highlight the QSLs and the HFT, are shown in the lower row of Figure 2 for comparison. Q was calculated following the procedure extensively described in Paper I. This comparison reveals that both current layers are clearly located along the QSLs, and not very far from the central axis of the HFT (defined as the narrow volume where Q is close to its maximum, shown in red in Figure 2). The horizontal layer is slightly shifted from the HFT toward negative x , while the vertical layer is more shifted from the HFT, toward low z . These shifts are a natural consequence of the fact that the area, covered by the twisting motions at $z = 0$ for $t < t^*$, did not include the footpoints of the central axis of the HFT. As argued in Paper I, even though any footpoint motion is expected to generate electric current layers along QSLs, being preferentially thinner and more intense around HFTs, the precise shapes and locations of these layers are still controlled by the form of the line-tied motions.

3.2. ORIGIN OF THE COMPLEX QSL DEFORMATION

This dual deformation of the QSLs naturally finds its origin in the early twisting motions which stressed the initial potential field configurations for $0 < t < t^*$. Referring to the color-coding of field lines shown in the upper row of Figure 2, the QSL motions naturally resulted in the displacement of red-type (resp. cyan-type) field lines mostly in the y (resp. x) direction. This was ensured by the 2D horizontal motions prescribed at their footpoints, which propagated along the field lines, thanks to quickly damping Alfvén waves. Both types of field lines also expanded toward higher z . This motion was due to local increases of magnetic pressure, at low altitude in the inner bipole, thus leading to a slow rise of the twisted volume. This expansion can also be physically interpreted as the consequence of the repulsion between the volume electric currents which developed in the domain and the surface currents which developed in the infinitely conducting plane at $z = 0$. These latter currents are equivalent to those produced by so-called “image currents”, which can artificially be placed at $z < 0$ so as to preserve $b_z(z = 0)$, as in the models of van Tend and Kuperus (1978).

We can make an analogy between the present QSLs with their HFT (projected onto 2D planes with fixed y , see Figure 2) and 2D separatrices with their null point (formed in classical quadrupolar configurations). While true separatrices are known

to separate a magnetic field in well-defined connectivity domains, QSLs do not. However, the 2D analogy allows us to consider quasi-connectivity domains which help to understand the time evolution of the 3D field lines. In this context, the red-type (resp. cyan-type) field lines are located in the central (resp. in a lateral) “quasi-connectivity domain” and they move toward the black-type (resp. green-type) field lines, the latter being located in the overlaying (resp. the other lateral) “quasi-connectivity domain”. This naturally forms a horizontal (resp. vertical) current layer at the null point in the case of separatrices, or near the HFT in the case of QSLs. Of course there is a competition between the horizontal motions and the vertical expansions in 3D, because of the non-local response of the magnetic field to boundary motions. The shapes and locations of current layers are therefore not easy to predict in general, using 2D analogies.

It is noteworthy that the formation of two nearly orthogonal narrow current layers at the same time in the QSLs was caused by a very simple and relatively weak torsional displacement of field line footpoints. This cannot happen in 2D and 2.5D geometries involving separatrices, in which only one single current sheet can be generated at the intersection of the separatrices when line-tied motions are prescribed (see *e.g.* Low and Wolfson, 1988). We conjecture that in 3D, complex deformations of QSLs are easy to obtain in general. This is typically expected, for example, when the boundary motions expand a “quasi-connectivity domain” in one region and shrink it in another region. Still, some conditions can prevent the formation of various current layers in QSLs. One example is 3D magnetic field configurations and 2D footpoints motions which maintain special symmetries during time, as done in many previously published numerical experiments, and as naturally set-up in laboratory experiments. One single current layer is also expected to be formed when a “quasi-connectivity domain” is dominantly expanded by the boundary motions. The set-up of our translation simulations in Paper I falls into this case. In general for 3D configurations, since the photospheric flows are not expected to have any relationship with the QSL locations, a complex pattern of current layers is expected along the QSLs, though it must depend on how the “quasi-connectivity domains” are evolved by the flows.

3.3. UNDRIVEN COLLAPSE OF THE CURRENT LAYERS

At $t = t^*$, in the regions where extended electric currents exist, the deviation from the force-freeness as estimated by $\epsilon = |\mathbf{j} \times \mathbf{b}|/|\mathbf{j}| |\mathbf{b}|$ is typically $\epsilon \sim 0.1\%$. Thus the magnetic field configurations are nearly force-free, i.e. $\mathbf{j} \sim \alpha \mathbf{b}$ with α defined in Equation (6). The weak non force-freeness comes from residual Lorentz forces associated with small wave-number Alfvén waves. These waves were traveling along the magnetic field lines so as to allow the magnetic field to adjust progressively to the continuous twisting motions that existed at $t < t^*$. Thanks to the viscous filter, these waves damp in a few Alfvén time scales during the MHD relaxations.

In the QSLs, especially within both current layers described above, the non force-freeness peaks at $\epsilon \sim 1 - 2\%$. Even if this shows that the QSLs are not so far from being force-free, the related Lorentz forces are there the strongest in the whole domain. These forces do not decrease very quickly in time. They are the cause of magnetic reconnection in both current layers. All around the QSLs, the Lorentz force vectors are all directed more or less perpendicular to the QSLs and they have converging patterns toward the QSLs. So the related current layers tend to collapse under the action of these forces, without any boundary driving. Figure 3 shows 1D cuts along z , at several times during one of the MHD relaxations, of various physical quantities across the horizontal current layer located in the vicinity of the HFT (see Figure 2). The plots stand for $\Phi = 150^\circ$ and $\eta = 10\eta^*$. The same kind of plots can be produced along x for the vertical current layer, and for $\Phi = 120^\circ$. The double-peaked Lorentz forces \mathbf{f} along the z axis result in the development of

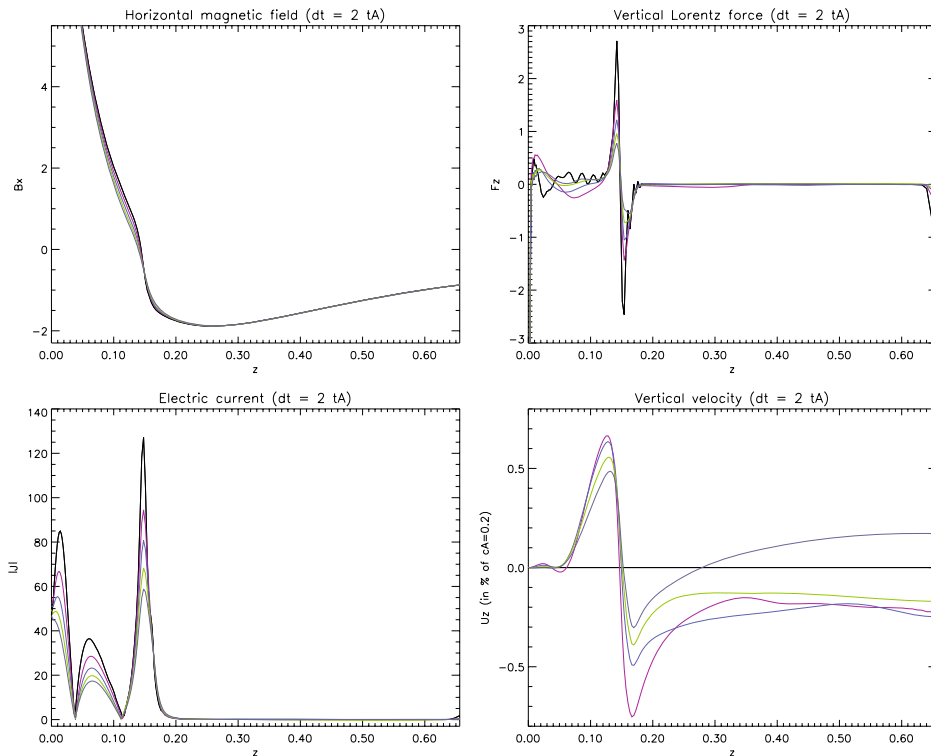


Figure 3. Temporal variation of 1D cuts along z at $(x; y) = (-0.003; 0.07)$ of various physical quantities, during the resistive relaxation of the configuration $\Phi = 150^\circ$, using $\eta = 15 \times 10^{-6}$. *Upper-left:* the x component of the magnetic field \mathbf{b} . *Lower-left:* the magnitude of electric currents \mathbf{j} . *Upper-right:* the z component of the Lorentz force $\mathbf{j} \times \mathbf{b}$. *Lower-right:* the z component of the velocity \mathbf{u} in units of $c_A(t=0) \times 10^{-2} = 2 \times 10^{-3}$. On each panel, each quantity is plotted for $t = t^* + (0; 2; 4; 6; 8)$ in (black; pink; blue; green; grey).

sub-Alfvénic pinching motions, in and around the current sheet. Their small speed is a natural result of the weak ϵ values. These motions quickly reach a larger extension along z than the width of the current sheet, because of the response of the distant magnetic fields to the local deformation of the current layer, which typically occurs on an Alfvén time scale (and probably also because of the viscous diffusion). The undriven self-collapse of the current sheet locally increases the resistive term in Equation (2), which in turn triggers magnetic reconnection. Its 3D nature is analyzed in Section 4.

This behavior can be related to 1D current layer models (*e.g.* Harris current sheets). Let us consider a magnetic field distribution along one axis z , which only has a component along x direction: $b_x(z) = \tanh(z)$. A current layer exists around $z = 0$. The Lorentz force \mathbf{f} reduces to the magnetic pressure force along z , which is $f_z \propto -\partial_z b_x^2$. This term shows two peaks of opposite signs which, in ideal MHD, must result in a fast implosion of the current layer, within a finite time (Forbes, 1982). This collapse can be slowed (or halted) by the inclusion of large enough plasma pressure, or magnetic field component perpendicular to the $(x; z)$ plane, or resistivity (Forbes, 1982; McClymont and Craig, 1996). Even if there is an analogy between our 3D MHD relaxations and this 1D current sheet model (see Figure 3), there is also a significant difference. This difference is due to the weak ϵ values in the MHD relaxations. There, the double-peak profile of \mathbf{f} is in fact a combination of several magnetic field derivative terms, whose individual amplitudes are typically 20–40 times as large as the result of their sum. The Lorentz forces around the 3D QSL current layers are thus relatively weaker than in 1D Harris current layers, because of the existence of several magnetic field components which ensures a nearly force-free evolution during line-tied motions.

3.4. CRITICAL η FOR QUASI-STEADY-STATE RECONNECTION

It is physically and numerically interesting to understand which conditions can prevent the current layer from collapsing to a zero thickness, *a fortiori* beyond the mesh resolution. Since our MHD relaxations are in zero- β , plasma pressure cannot counteract this collapse. At the first order, the slowness of the collapse (due to the low ϵ values) permits the magnetic field component perpendicular to the current sheet to evacuate most of the stress that is generated within the current layer by the collapse, toward large distances, thanks to Alfvén waves. So flux pile-up and therefore magnetic pressure forces within the current layers that could oppose the collapse are not as efficiently created as in 1D models (*e.g.* Forbes, 1982). So at the first order on relatively short time scales, only resistivity can prevent the collapse of the current layer.

In an open medium, the minimum resistivity which has to be considered to prevent the collapse is the one that leads to a steady state (or stationary) solution. However, no real steady-state regime can be reached in our MHD relaxations,

because the line-tying constraint at $z = 0$ prevents magnetic flux from rising indefinitely toward and into the QSL current layer at $z > 0$. If one considers the evolution of horizontal current layers, the rise of magnetic field lines along z must lead to an increase of the magnetic tension, which points downward along z , so the tension will eventually halt this rise. Still, the slow amplitude of the pinching velocities along z can allow a quasi-steady-state regime to be satisfied for many Alfvén times, thus allowing to derive the critical η_c value as follows.

Let us analyze a horizontal current layer, in which the strongest field gradients are in the z direction. Let us consider, at first order, that the current layer is 1D. In this approximation, the horizontal derivatives are zero ($\partial_x = \partial_y = 0$), the inflow velocities are vertical ($u_x = u_y = 0$) and the magnetic field is horizontal ($b_z = 0$). Under the steady state condition ($\partial_t = 0$ and $\eta = \eta_c$) and for any horizontal magnetic field component $b_i = b_x$ or b_y , Equation (2) then reduces to:

$$-b_i \partial_z u_z + \eta_c \partial_z^2 b_i = 0. \quad (7)$$

Its dimensional analysis results in:

$$\eta_c = u_i \delta^2 / L_z, \quad (8)$$

where u_i is the maximum amplitude of the inflows, L_z is their length scale and $\delta \sim \alpha^{-1}$ is the scale length of the magnetic field gradients in the current layer (i.e. the width of the current layer at FWHM). For both magnetic field configurations and at early times, u_i weakly depends on η . This is natural, since we have seen that the inflow is due to an ideal MHD process. These speeds are typically $u_i \sim 10^{-3} \sim 0.5\% c_A$. After a few Alfvén times, u_i becomes different because subsequent magnetic reconnection pulls magnetic flux away from the current layer. So reconnection decreases the magnetic pressure, thus increasing the pinching pressure forces. We do not consider these variations at first order.

From Figure 3, one can estimate $\delta \sim 0.02$ and $L_z \sim 0.15$. Equation (8) then results in $\eta_c \sim 3 \times 10^{-6} \sim 2\eta^*$. Almost the same result can be reached for the vertical current layer and for $\Phi = 120^\circ$. This estimation actually fits quite nicely the results of our relaxations using different η values. On one hand, we find quasi-steady states for $t < t^* + 40$, using $\eta = 3\eta^*$. On the other hand, the current layers collapse below the mesh resolution for $t < t^* + 15$ using $\eta = \eta^*$. Finally, they rapidly diffuse for $\eta = 10\eta^*$. These results are further described below.

4. Local Dynamics and Global Oscillations

4.1. RECONNECTION JETS AND η -DEPENDENCE

The undriven collapse of the narrow current layers described in Section 3.3 and shown in Figure 3 results in an enhanced magnetic diffusion and therefore in magnetic reconnection. The reconnecting current layers are at the location of the

strongest currents along the QSLs (see α maps in Figure 2). These currents are nearly aligned with the magnetic field (see ϵ values in Section 3.3). So the strongest field-aligned resistive electric fields ($E_{\parallel} = \eta J_{\parallel}$) are co-spatial with the 3D reconnecting layers in our QSL configurations. Our calculations thus nicely follow the conditions for general magnetic reconnection in 3D (Hesse and Schindler, 1988).

As viewed in Figure 4, in $(x; z)$ planes for $y = \text{constant}$ the magnetic reconnection is associated with the formation of sub-Alfvénic plasma jets. These jets diverge from the diffusive layers, and their velocity component along y has about the same amplitude as those in the $(x; z)$ plane. For $\Phi = 150^\circ$ and $\eta = (1; 3; 10)\eta^*$, the maximum velocities of the jets during the first few Alfvén times are $u_J = (0.45; 0.85; 1.75)\% c_A$, respectively. These jets are associated with inflow velocities $u_i \sim 0.5\% c_A$ which are nearly independent of η (see Section 3.4). The velocities given above were normalized to the homogeneous initial Alfvén speed $c_A = 0.2$ given in Section 2.1. The latter indeed gives a good approximation of the total

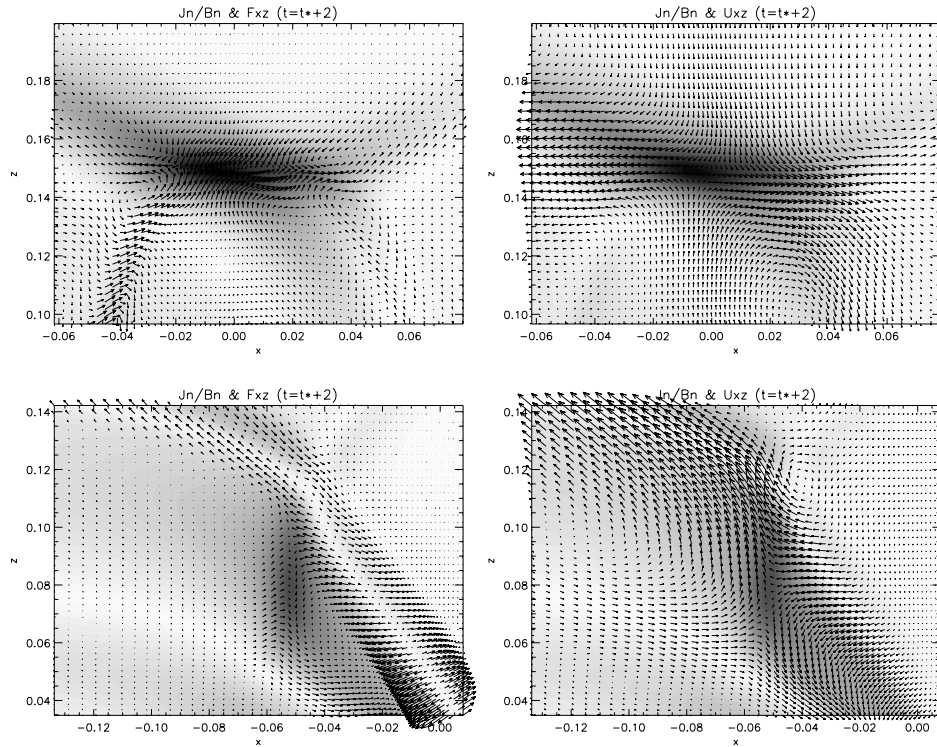


Figure 4. Close-up around the narrowest current layers shown in Figure 2 at $t = t^* + 2$, for $y = 0.07$ (upper row) and $y = -0.12$ (lower row). The greyscale color coding correspond to $j/b \sim |\alpha|$. Arrows correspond to 2D vectors of the fluid velocities (right column) and of the Lorentz forces (left column) in the $(x; z)$ plane. The arrow lengths are proportional to the norm of their corresponding vector field in the 2D plane.

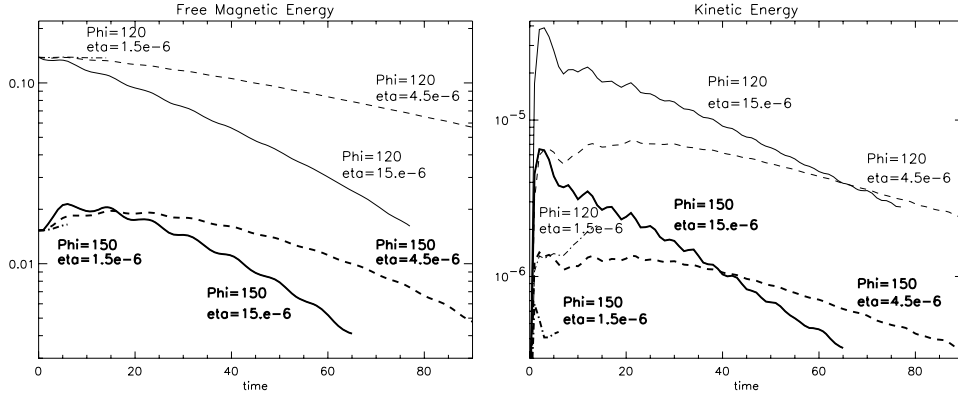


Figure 5. Free magnetic and kinetic energies during the resistive relaxations. The *thick* (resp. *thin*) curves stand for the configuration $\Phi = 150^\circ$ (resp. $\Phi = 120^\circ$). *Continuous*; *dashed*; *dash-dotted* curves stand for resistive relaxations using $\eta = \eta^*$; $3\eta^*$; $10\eta^*$, respectively.

space-varying Alfvén speed for $t > t^*$ since it only varies between 0.18 and 0.23 in all our relaxations. For both magnetic field configurations (i.e. both Φ values), the sub-Alfvénic outflow velocities are a monotonic function of η and the maximum values for the total kinetic energies naturally follow the same trend.

During the reconnection, the gradual diffusion of the magnetic fields naturally leads to a decrease of the magnetic energies E_b . Meanwhile, the slow decay of the current layers progressively results in slower and less extended reconnection jets, so that the kinetic energies E_k also decrease in time. Plots of the free magnetic energy δE_b (as defined in Section 2.2) and of E_k as a function of time are shown on Figure 5 for all six MHD relaxations. For both Φ , these decays in energy are mostly obvious during relaxations using $\eta = 10\eta^*$. Once reconnection has started, the kinetic energies remain nearly constant for several tenths of Alfvén times when using $\eta = 3\eta^*$. During this plateau, the current layers very slowly decay. It is also worth noticing that for $\eta = \eta^*$, the calculations rapidly break down. This particular behavior is due to the collapse of the current layers, during which reconnection jets amplify, until the currents become unresolved, which leads to numerical instabilities quickly halting the calculations. These different behaviors, for various η , nicely follow the estimations reported in Section 3.4.

Testing whether or not the classical Sweet-Parker reconnection regime in 2.5D exists in the 3D systems considered in this study is not straightforward. Indeed, it is hard to find a guide field direction precisely in the HFT, which is needed to define the local “perpendicular” Alfvén speed $c_{A\perp}$, that is supposed to be reached by the reconnection jets in this regime. Let us focus on the horizontal current layer which exists near $y = 0.07$ for $\Phi = 150^\circ$. Since the HFT is primarily oriented in the $(y; z)$ plane (as seen in the top-right panel of Figure 2) and since b_x is the magnetic field component which has the strongest gradients in this layer, let us assume the crude approximation (as in Section 3.3) that the horizontal current layer can be treated

by a model in which b_x is the only component of the magnetic field which is being diffused along the z axis, and that the reconnection jets are primarily oriented along the x axis. In this simple approximation, $c_{A\perp} = \sqrt{b_x^2/\rho}$. Out of the diffusive layer $c_{A\perp} \sim c_A \sim 0.1\text{--}0.2$ (in the middle of this layer, this quantity naturally falls down to 0 since there b_x changes sign, as seen in Figure 3). As mentioned above, the outflow velocities in the reconnection jets are therefore $u_J \ll c_{A\perp}$. This shows that the 2.5D Sweet-Parker reconnection regime is not reached in our 3D relaxations. This may be due to several reasons. Firstly, the diffusion time of the current layers may be shorter than the time required for them to adapt their shapes so as to reach this regime. This is not unlikely since no external driving was imposed during the relaxations and since the inflow velocities were fixed by the Lorentz forces in the current layers (see Section 3.3). Secondly, the use of a too high viscous filter and of a too coarse mesh (so of a too low magnetic Reynolds number), both during the driving and the relaxation phases, may have prevented the current layer to evolve toward this standard regime. Understanding this issue, which is not the primary topic of this paper, would require further analyses.

4.2. BOUNDARY-DRIVEN OSCILLATIONS ON LARGE-SCALES

Two peculiar features appear on Figure 5: damped oscillations of δE_b and E_k superposed on their global decrease in time (for both Φ) and rises in δE_b at small times (for $\Phi = 150^\circ$ only). Both have the same origin.

The energy oscillations visible in Figure 5 could, *a priori*, be attributed to physical non force-free magnetic field perturbations which naturally generate new Alfvén waves for $t > t^*$, since all velocities were reset to zero at $t = t^*$. Even though this effect must exist, it cannot explain the energy oscillations of Figure 5 because (i) the frequency of the oscillating component of E_k is twice that of δE_b and (ii) using the dispersion relation for Alfvén waves, they should correspond to spatial frequencies ~ 1 , which is not typical of the length of the previously twisted and now reconnecting field lines.

In fact, these oscillations rather seem to be due to numerical boundary effects, in the weak field regions, as illustrated in Figure 3, since residual Lorentz forces exist near the open boundaries. These forces are due to artificial small electric currents extending two to three grid points from the boundaries into the domain. These currents are generated from our numerical prescriptions of so-called “open” boundaries with non-zero magnetic field gradients using ghost-cells (see Paper I). These artificial forces first result in weak implosion-type motions toward the flux concentrations, followed by weak diverging motions toward the open boundaries when magnetic pressure has sufficiently built-up in the domain so as to counteract the early implosion. This process repeats itself, thus leading to weak oscillations in the whole numerical domain, during tens of Alfvén times. Since new flux can enter into the numerical domain through the open boundaries, δE_b can increase

(resp. decrease) when inflows (resp. outflows) are present. Its temporal frequency is therefore that of the global oscillations. E_k has a maximum both during the inflow and outflow, which explains why its temporal frequency is twice that of δE_b . The initial rise in δE_b in each relaxation for $\Phi = 150^\circ$ is due to the initial implosion, which is faster than the subsequent ones, thus bringing more magnetic energy density into the domain from the open boundaries. Even though the same process occurs for $\Phi = 120^\circ$, it does not lead to an increase of the total magnetic energy, because its evolution is there dominated by the resistive energy decrease. The initial implosion and the first following oscillation are visible on velocity and Lorentz force plots in Figure 3, at large z above the narrow current layer.

Performing some numerical experiments, we found that setting $\eta = 0$ near the boundaries reduced this phenomenon, but it did not completely suppressed it. In the present relaxations, these oscillations do not affect the reconnecting regions, probably because the magnetic field and density are there stronger.

5. Three-Dimensional Slip-Running Reconnection

5.1. FIELD LINE SLIPPAGE IN OPPOSITE SENSES ALONG QSLs

In spite of the fact that the MHD relaxations are performed using $\mathbf{u}(z=0) = \mathbf{0}$ and $\eta(z=0) = 0$, some magnetic field lines do not remain anchored at the same position in the line-tied plane at $z=0$. Figure 6 shows how such field lines gradually slip along one another. Each of them is integrated from a fixed footpoint position in the negative polarity, in the vicinity of a QSL. Their conjugate footpoints all move along the same arc-shaped trajectories at $z=0$, from the positive polarity of the outer bipole to that of the inner bipole, or in the opposite direction, depending on the field line. The same process occurs more-or-less (but not exactly) symmetrically for field lines with fixed footpoints in the positive polarity.

While field line slippage has already been reported in MHD simulations of magnetic reconnection in a straight and stressed HFT (Pontin *et al.*, 2005) and in simulations of prominence merging due to shearing dipoles (DeVore, Antiochos, and Aulanier, 2005; Aulanier, DeVore, and Antiochos, 2006), the present calculations reveal that the arc-shaped trajectories on both sides of inversion line correspond to the intersection of the QSLs with the line-tied plane (these arcs are shown in Paper I). Further analysis reveals that during their gradual slippage, field lines cross the narrow volume of the QSLs in the domain. Therefore, QSLs are the global and fully three-dimensional generalization of the 2.5D “magnetic flipping layers” identified by Priest and Forbes (1992b).

The side-views along the y axis shown in the left column of Figure 6 are reminiscent of standard 2D reconnection models with NP separatrices in quadrupolar configurations. The red-type field lines (initially located in the central

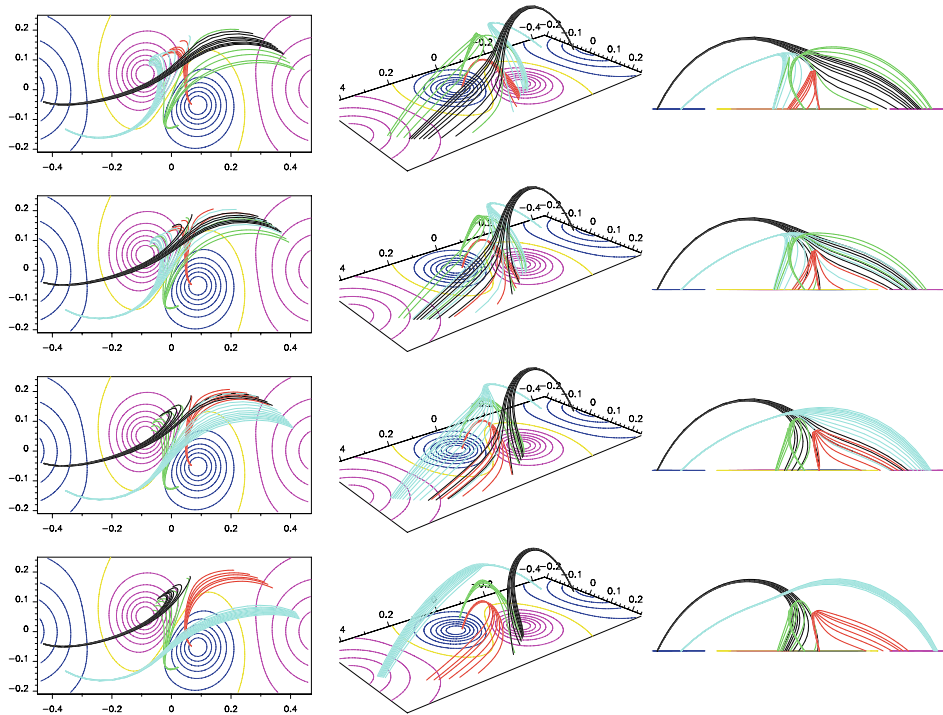


Figure 6. Slip-running field lines, for $\Phi = 150^\circ$ and $\eta = 15 \times 10^{-6}$, shown at $t = t^* + 0, +3, +10, +30$, going down from the first row. The contours of $b_z(z = 0)$ are the same as in Figure 1 and the color-coding of field lines is the same as in Figure 2. At every time, each field line is integrated from the same footpoint position at $z = 0$, in the negative magnetic polarity, near the intersection of the QSL with the $z = 0$ plane. For a given field line color, the fixed footpoints are placed along a very short line-segment, which is orthogonal to QSL. The *left, middle* and *right* columns show top (along z), projection and side (along y) views respectively. [This figure is available as GIF animations in the electronic version of *Solar Physics* – see Appendix.]

“quasi-connectivity domain”) reconnect with the black-type ones, (initially located in the overlaying “quasi-connectivity domain”), gradually exchanging their connections through field line slippage (thus forming new field lines in both lateral “quasi-connectivity domains”). During this process, both types of field lines slip along each other along QSLs. The same process occurs at the same time, for the cyan- and green-type reconnecting field lines, but in this case the pre-reconnection field lines are both located in the lateral “quasi-connectivity domains”. So reconnection proceeds in two opposite senses at the same time in the QSLs.

The field lines drawn in Figure 6 are of the same type as those drawn in Figure 2. For a given ensemble of field lines (of a given color in Figure 6), the line-segment defined by their fixed footpoint positions, in the negative polarity, was chosen so as to cross the intersection of the QSLs with the line-tied boundary, close to the

footpoint position of the field line of the same color shown in Figure 2. The red and black (resp. cyan and green) field lines are thus closest to one another on both sides of the horizontal (resp. vertical) current layer (shown in Figures 2 and 4). It is interesting to notice how the simple and weak twisting of one single polarity in a four flux and bipolar system naturally produces such a complex reconnection and field line slippage patterns.

5.2. SLIP-RUNNING REGIME

The tracking of individual field line footpoints on Figure 6, especially between $t = t^*$ and $t^* + 3$, suggests that some of them slip at velocities of the order of the Alfvén speed along the arc-shaped QSL. These displacements do not correspond to real bulk motions, but to the rearrangements of the global field lines as a result of reconnection. Indeed, the magnetic field is locally and gradually diffused within the current layers. This occurs, at a given time, where the field lines have the strongest gradients of connectivity, within the QSLs and near the central axis of the HFT. In such conditions, field lines must naturally exchange their connectivities with that of their neighbors, in a continuous way. This is the physical origin of field line slippage in QSL reconnection, as already reported in past MHD experiments referred to in Section 1.

This continuous change of connectivity during reconnection must be fast when the QSLs/HFT are thin, since by definition, neighboring field lines there have strong gradients of connectivity. When this process occurs at (super) Alfvénic speeds, magnetic field lines can change their connections on time scales far shorter than the travel-time of Alfvén waves along them.

Let us describe what happens in this case, with a field line that has two initial footpoint positions labeled A and B . Before reconnection, when an Alfvén wave is emitted (or reflected) from the footpoint A , it travels to B and it is reflected back to A over a time scale of $2t_A$, thus bringing to A the information that the connectivity of the field line is $A - B$. When it is reflected from A and as reconnection starts, the wave must then gradually change its direction of propagation, following the fast slippage of the field line along which it travels. Meanwhile the conjugate footpoint of the field line quickly slips from its initial position B to a new distant position C . So after a time scale of t_A , the wave reaches the conjugate footpoint of the field line at C , from which it is reflected back to A along the now fixed field line. Therefore, over a time scale of $2t_A$ the wave only carries back to A the information that the field line has changed its connectivity from $A - B$ to $A - C$. So on MHD time scales, the footpoint A has no way to “know” that the field line has slipped in a continuous way. The system must therefore respond to any MHD perturbation as if the field line had changed its connectivity abruptly, which is exactly what happens when reconnection occurs at true separatrices. QSLs can thus physically behave as true separatrices on MHD time scales.

We define this regime as *slip-running reconnection*. This process is an intermediate between two previously recognized regimes: first, abrupt field line reconnection when true separatrices exist (i.e. with infinite slippage velocity) and second, mild and slow field line slippage during magnetic field diffusion.

Naturally, the exact definition of the slippage velocity is ambiguous, since it depends on which fixed position is selected in the domain from which a field line is integrated at different times. Choosing a position within the reconnecting current layer, which approximately evolves in time accordingly with the local plasma velocity (i.e. following a plasma element), results in the very asymmetric slippage of both footpoints of the field line. In general, one footpoint weakly moves whereas the other one slips in a very similar way as if the field line was integrated from a fixed position at the $z = 0$ boundary. So the definition of the slip-running reconnection regime seems not to be very sensitive to this issue. Even though considering field lines which are integrated from moving plasma elements may be more meaningful physically, in the following we keep analyzing field lines that have one footpoint fixed at the line-tied boundary, because this method more clearly illustrates the slippage from one “quasi-connectivity domain” to another.

5.3. SLIPPAGE VELOCITY AS A FUNCTION OF η AND Q

Figure 7 shows the evolution in time of selected field lines with fixed footpoints in the negative polarities, so as to measure the slippage velocities of their conjugate footpoints along the QSLs, in the positive polarities. The relaxations there show that the slippage of a given field line is continuous, but not uniform in time (mostly for $\Phi = 150^\circ$): the slippage velocities have a well defined maximum in time, between two slower phases. Other field lines rooted in the vicinity of the QSL (as shown in Figure 6) have the same behavior, except that their faster slippage does not occur at the same time. Fast field line slippage is therefore also a continuous process, which lasts for many Alfvén times after $t = t^*$, as long as the reconnecting layers are not fully dissipated.

The maximum slippage velocity occurs when the footpoints transit from one positive flux concentration to the other, which in our models corresponds to the thinnest portions of the QSLs, close to the axis of the HFT. The relaxation for $\Phi = 150^\circ$ and $\eta = 10\eta^*$ clearly shows that the cyan (resp. red) field line moves super-Alfvénically (resp. slightly slower than the Alfvén speed) in this region, at $t \sim t^* + 1.5$ (resp. $\sim t^* + 2.5$). There, all reconnecting field lines are in the slip-running regime. For $\Phi = 150^\circ$ and $\eta = 3\eta^*$, only the cyan field line is slip-running (its footpoints moves at the Alfvén speed at $t \sim t^* + 4.5$). For $\Phi = 120^\circ$ and $\eta = 10\eta^*$, the field line slippage is much slower, in a rather diffusive-like regime, even though the current layers have approximately the same widths as for $\Phi = 150^\circ$.

We come to the conclusion that Q is the main factor that determines the conditions for slip-running reconnection, although resistivity also plays a role. For

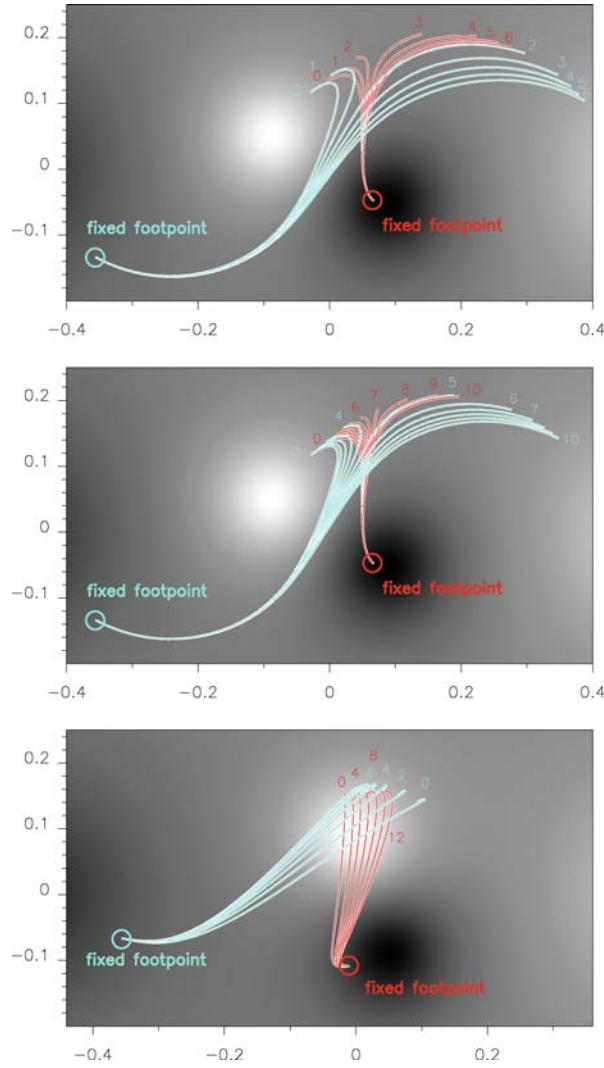


Figure 7. Time evolution of two slip-running field lines with fixed footpoints in the negative polarities. The greyscale color coding shows $b_z(\tau = 0)$ and the color-coding of field lines is the same as in Figure 2. Three relaxation runs are shown: for $\Phi = 150^\circ$ and $\eta = 15 \times 10^{-6}$ (*top panel*); $\Phi = 150^\circ$ and $\eta = 4.5 \times 10^{-6}$ (*middle panel*); $\Phi = 120^\circ$ and $\eta = 15 \times 10^{-6}$ (*bottom panel*). The fixed field line footpoints are indicated by *circles*. The time interval between each plotted field line is the same in any given panel. It is equal to 1 (resp. 2) for $\Phi = 150^\circ$ (resp. 120°).

comparison, the maximum Q in our configuration $\Phi = 120^\circ$ is of the same order as the one which was reached in the calculations Pontin *et al.* (2005) after large deformations of the HFT (see Gasgaard *et al.*, 2003). We thus also conclude that very strong deformations of an initial configuration that does not already contain very narrow QSLs are required so that the diffusion of narrow current layers

permits slip-running reconnection. Magnetic configurations that initially possess narrow QSLs are most favorable for the occurrence of slip-running reconnection.

At the line-tied boundary, the fast slippage velocity along the QSL v_{\parallel} can be related with the displacement of the QSL, which occurs at a slower velocities v_{\perp} orthogonally to its elongated direction. This transverse displacement results from the reconnection process, as further described in Section 5.4. Let us consider a field line with a fixed footpoint initially located on one edge of an arc-shaped QSL. As the QSL shifts in position during magnetic reconnection, the fixed field line footpoint gradually moves inside the QSL. When the QSL has shifted in position by its full width d_{\perp} , the conjugate footpoint of the field line, on the other side of the inversion line, must have slipped all the way along the other arc-shaped QSL of length d_{\parallel} . So the ratio between the maximum slippage velocity and the transverse QSL velocity should be of the order of:

$$\frac{v_{\parallel}}{v_{\perp}} \sim \frac{d_{\parallel}}{d_{\perp}} \sim \sqrt{Q}. \quad (9)$$

Observationally, the field line slippage velocity could be predicted from the transverse displacements of flare ribbons (which correspond to the footprints of the QSLs in the chromosphere, see *e.g.* the review of Démoulin, 2006) as observed in $H\alpha$ or in EUV, and from the squashing degree calculated from force-free magnetic field extrapolations of photospheric magnetograms.

5.4. RELAXATION OF CURRENTS AND QSL DE-STRETCHING

The resistive diffusion of current layers within the domain is associated with changes in electric currents at the line-tied boundary. The latter also change shape and slowly decrease in amplitude. Such changes at $z = 0$ are shown in the top panels of Figure 8 for $\Phi = 150^\circ$ and $\eta = 10\eta^*$. These variations are not a direct consequence of resistivity at $z = 0$, since there η is set to zero and b_z is fixed in time. These changes are rather due to the gradual rearrangement of field line connectivities so as to diminish their relative stress. They are both due to fast slip-running reconnection in the QSLs and to slow magnetic field diffusion in the quasi force-free extended currents (see Figure 3), as a direct consequence of our uniform resistivity at $z > 0$. Figure 8 also shows a sample of slip-running field lines (with a different color convention as in Figures 2 and 6), whose fixed footpoints are located in the regions where the current layers shift in time.

During the relaxations, the gradual diffusion of the current layers lead the QSLs to lose the deformations that the line-tied motions induced at earlier times (see Section 3.1). Doing so, the QSLs also gradually shift in space. These shifts occur all along their lengths in the domain, down to the line-tied boundary as shown in the lower panels of Figure 8. This process is the 3D generalization of the displacement of separatrices to different Clebsch variable values during 2.5D null point reconnection, as analyzed by Antiochos, Karpen, and DeVore (2002). Doing the

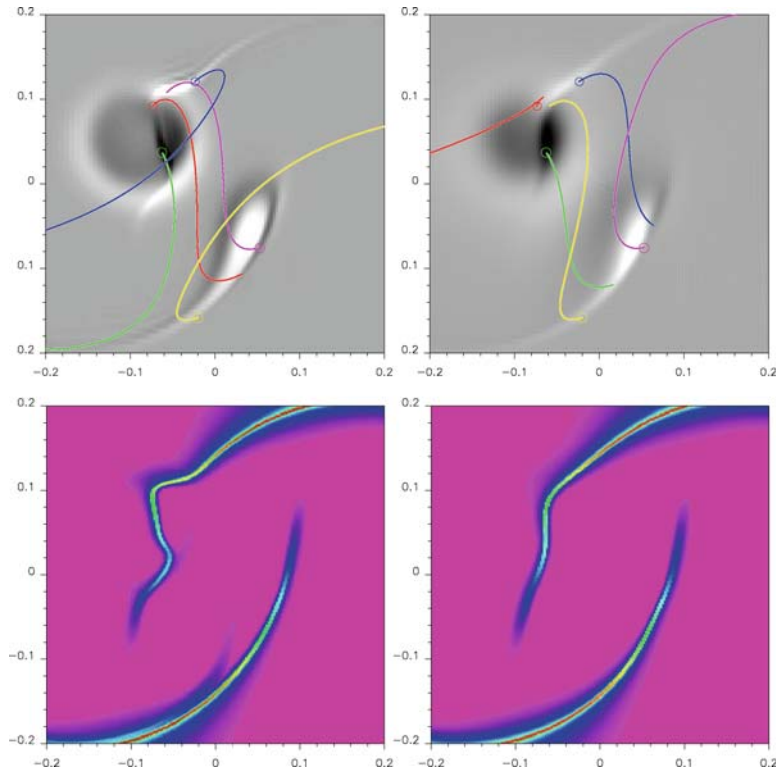


Figure 8. *Top row:* Slip-running field lines overlaid on greyscale images of the vertical electric currents on the line-tied boundary $J_z(z=0)$ for $\Phi = 150^\circ$ and $\eta = 15 \times 10^{-6}$, at $t = t^*$ (*left panel*) and $t = t^* + 20$ (*right panel*). The greyscale values range from $J_z = -500; +250$ (resp. $-250; +125$) on the *left panel* (resp. *right panel*), from *black to white*. One footpoint of each field line is fixed in time, as indicated by circles. *Bottom row:* Corresponding maps of the squashing degree $Q(z=0)$, which show the intersections of the QSLs with the line-tied boundary. The (*red; yellow; green; cyan; blue; pink*) colors stand for $Q = (10^8; 3 \cdot 10^6; 10^5; 5 \cdot 10^3; 50; 2)$.

same 2D reconnection analysis for different fixed position along the y axis (see Section 5.1), and considering the color coded field lines of Figures 2 and 6, one finds that the reconnection of the red and black (resp. cyan and green) field lines, at the horizontal (resp. vertical) current layer, should lead to a shrinkage (resp. an expansion) of the central lower “quasi-connectivity domain” along x , for $y = 0.07$ (resp. -0.012). Indeed, the associated field line slippage will transfer the red (resp. green) field lines to a lateral (resp. the central) “quasi-connectivity domain” (see Figure 6). The de-stretching of the QSLs (shown in the lower panels of Figure 8) almost exactly shows this behavior.

Only small portions of the QSLs, located on the edge of the strongest return currents move in the opposite directions as what is predicted by the 2D analogy (i.e. around $(x; y) \sim (-0.02; 0.12)$ and $(x; y) \sim (-0.1; -0.04)$ in the positive polarity

of the inner bipole). The slip-running dark blue field line shown in Figure 8 is in one of these two regions. Since these regions are at the continuous transition between “quasi-connectivity domains”, it is natural that the 2D analogy fails to predict their behavior. In such regions in general, a detailed analysis of the 3D distribution of the Lorentz forces is therefore required to understand in what sense reconnection will take place.

It is also worth noticing that as the QSLs shift position during the reconnection, electric currents shift with them. As for separatrix displacements (or slip-running field line motions), QSL de-stretching is not a physical motion, therefore the electric current shifts cannot be a result of the advection of slowly diffusing current layers. They are rather due to the gradual reformation of current layers in the evolving QSLs, thanks to the reconnection induced motions in the domain and connectivity rearrangements at the line-tied boundary. This by-product result shows that narrow current layers can naturally be generated along thin QSLs, not only with any type of line-tied motions (as shown in Paper I), but also with plasma motions above the line-tied boundary. We believe that this does not depend on the origin of these motions, which could either come from ideal instabilities, reconnection jets, etc. This is rather an intrinsic property of QSLs, which is a consequence of their drastic mapping changes.

Finally, Figure 8 obviously shows that our resistive relaxations do not evolve the magnetic field configuration toward a linear force-free state ($\alpha = \text{constant}$), even after a hundred Alfvén times (note that the diffusion time is ~ 2700 Alfvén times for a length scale $L = 0.2$ and for $\eta = 10\eta^*$). This property has been noted in many MHD experiments for solar physics. It is in contradiction with the predictions of Taylor (1974) that any magnetic field configuration must gradually relax to a linear force-free state, since it corresponds to the minimum energy for a given magnetic helicity (which is known to be nearly conserved for time scales much shorter than the global diffusion time scale). Amari and Luciani (2000) attributed this difference between Taylor’s conjecture and MHD simulations to the line-tying constraints, which may prevent turbulent reconnection from occurring everywhere in the magnetic field. This interpretation was further developed by Antiochos, Karpen, and DeVore (2002), who proposed that electric currents can only be redistributed in space thanks to reconnection in moving separatrices. The present results generalize the conditions for magnetic reconnection to QSLs.

6. Slip-Running Reconnection and Particle Acceleration

6.1. AMPLITUDE OF PARALLEL ELECTRIC FIELDS

We have seen in Section 4.1 that the reconnecting electric fields E_{\parallel} were the strongest in the QSL current sheets. In our non-dimensionalized units, $E_{\parallel} = \eta J_{\parallel} = 4.5 \times 10^{-4}$ in the quasi-steady state regime ($\eta = 3\eta^*$).

Considering a size of $L = 20$ Mm for the inner bipole (instead of 0.2), so that the width of the current layers are $\delta = 2$ Mm (instead of 0.02) and the size of the smallest grid point is $d = 150$ km (instead of 1.5×10^{-3}), then taking the maximum magnetic field in the photosphere to be $b_{\odot} = 1000$ G (instead of 35) so that the magnetic field in the current layers is $b = 60$ G (instead of 2), then the maximum current density is $J_{\parallel} = 2.3$ mA m $^{-2}$ (instead of 100). Also, considering a coronal Alfvén speed of $c_A = 10^3$ km s $^{-1}$ (instead of 0.2) so that the Alfvén time is $t_A = 20$ s (instead of 1), the resistivity for the quasi-steady state is $\eta = 2.2 \times 10^9$ m 2 s $^{-1}$ (instead of 4.5×10^{-6}). The physical parallel electric field, being expressed as $E_{\parallel} = \mu\eta J_{\parallel}$, is therefore $E_{\parallel} = 6$ V m $^{-1}$.

This value is much smaller than those estimated at large scales during intense solar flares, using transversal flare ribbon motions (Poletto and Kopp, 1986; Forbes and Lin, 2000; Qiu *et al.*, 2002), and even smaller than those required to accelerate particles to the observed range of energies (as modeled by *e.g.* Turkmani *et al.*, 2006; Dauphin, Vilmer, and Anastasiadis, 2006). Even though the present experiments imply that E_{\parallel} is quite small and that it decreases even further as η gets smaller, they do not preclude the existence of a re-increase of E_{\parallel} when η becomes even smaller. Indeed, very small η must lead to a stronger and faster collapse of the current layers toward very high current densities.

Such a parameter study though, is not achievable with the present resolutions which are too coarse to treat much sharper magnetic field gradients. Considering the spatial resolutions achievable by the presently existing computers, a direct use of large-scale MHD experiments as a background for quantitative particle acceleration models is therefore impossible. Qualitatively however, our MHD experiments can address the issue of particle acceleration, because they still predict where the strong E_{\parallel} can develop and how they can evolve in time.

6.2. MOTION OF HXR SOURCES ALONG FLARE RIBBONS

During intense solar flares, chromospheric ribbons as observed in H α and in EUV move apart from one another, as predicted by standard 2D reconnection models (*e.g.* Poletto and Kopp, 1986; Qiu *et al.*, 2002). Their separation velocities are of a few tens of km s $^{-1}$. Recent analyzes of Yohkoh/HXT and RHESSI observations have also revealed the common occurrence of hard X-ray (HXR) compact sources moving along the chromospheric ribbons, with rapid changes followed by relative stability, with peak velocities of several hundreds km s $^{-1}$ (Fletcher and Hudson, 2002; Krucker, Hurford, and Lin, 2003; Bogachev *et al.*, 2005).

These HXR motions along flare ribbons are often interpreted (in the frame of standard separatrix reconnection in 2.5D) as being due to the displacement of the reconnection layer in time, when the HXR sources move parallel to each other along the ribbons, or by the successive reconnection of more and more (resp. less and less) sheared field lines, when the HXR sources move antiparallel to each other toward

the ends (resp. the centers) of the ribbons. Let us discuss how QSL reconnection may also explain these HXR footpoint motions.

First, many confined and eruptive flares do not involve reconnection in separatrices, but rather in QSLs. In these cases, flare ribbons correspond to the intersection of the QSLs with the chromosphere (see *e.g.* Démoulin *et al.*, 1997 and the review of Démoulin, 2006), and the diverging motions of flare ribbons there correspond to those of the QSLs during the reconnection (as described in Section 5.4 in this paper). Second, when reconnection occurs in QSLs, regardless of the exact values for the reconnection electric field E_{\parallel} , one can reasonably assume that E_{\parallel} reaches its maximum value where the current layers are the thinnest, which is close to the HFT (where Q is maximum). Particles should therefore be accelerated to their highest energies close to the regions where field lines have the strongest gradients of connectivity. So their impact with the chromosphere, which produces HXR emission, should be located around the regions where $Q(z=0)$ is maximum, which are rather extended due to the HFT geometry (see the red regions in the lower panels of Figure 8). Third, we have shown in this study that QSL reconnection leads to field line slippage along the QSLs, so *a fortiori* along the intersection of QSLs with the chromosphere. So during the period of acceleration, particle impact along the chromosphere should also gradually move along the QSLs.

We therefore argue that the displacement of HXR emission along flare ribbons could be interpreted as a signature of field line slippage during magnetic reconnection in QSLs, which neither requires a displacement of the reconnection region along the ribbons, nor a drastic change of magnetic shear angle for the reconnecting field lines.

However, the details of this mechanism remain to be analyzed. Since both footpoints of a field line that is integrated from the diffusion region slip along the photosphere (as mentioned in Section 5.2) and since two reconnecting field lines have at least one footpoint which quickly slips, magnetic reconnection in QSLs can account for antiparallel HXR footpoint motions. Also, considering that HFTs may have complex deformations which lead to reconnection in opposite senses (see Figures 4 and 7), this process could also account for parallel HXR footpoint motions along two flare ribbons, and for (yet unobserved) crossing motions along one given ribbon. Finally, it is not sure that HXR footpoints can move all along the footprint of a QSL. Their motions may well be confined to the regions of highest Q values, i.e. at the footpoints of the HFT. The extent and the velocity of the HXR footpoint motion along a flare ribbon indeed must depend on three characteristic time scales: the duration of the particle acceleration in the diffusion region, their travel-time along the field lines and the time scale defined by the slippage velocity. If the particle-related time scales are far shorter than the field line-related ones, the HXR footpoints could be confined to the slowly moving footprints of the HFT. All these important issues are far beyond the scope of this study and they will have to be addressed in the future.

7. Conclusion

Mathematically speaking, quasi-separatrix layers and hyperbolic flux tubes (QSLs and HFTs) are not topological boundaries which separate distinct connectivity domains in three-dimensional magnetic field configurations, contrary to separatrices (and separators). QSLs/HFTs are rather geometrical objects which, when they are sufficiently thin (i.e. when their squashing degrees Q are large enough), form a sharp, but continuous, transition layer of magnetic field connectivity between different regions of the system. This mathematical difference in terms of continuous/discontinuous field line mapping a priori could (and for a long time did) lead to a strong under-estimation of their physical relevance for current sheet formation and diffusion as well as for magnetic reconnection. These physical processes are predominant features of solar flares, coronal heating and many other resistive phenomena in natural and laboratory strongly magnetized plasmas. We performed 3D resistive MHD numerical experiments, in the so-called cold-plasma approximation and using line-tied conditions at a single plane where the magnetic flux is the most concentrated (as in solar-like conditions). These experiments demonstrate that the physics involved at separatrices (formation of current layers and reconnection) is also present at QSLs.

We extended the conditions of current sheet formation in QSLs to any large-scale velocity perturbation, either being due to extended sub-Alfvénic line-tied motions or to plasma motions within the system driven by existing Lorentz forces. In terms of current formation, it follows that QSLs behave as separatrices, numerically when their thickness is smaller than the mesh resolution, and physically when their thickness is smaller than the dissipative scale-length. QSLs/HFTs can therefore play an equal role as separatrices/separators do, at least in the triggering of solar flares but also in the heating of the solar corona.

Our MHD relaxations clearly showed that 3D reconnection does occur in thin QSLs, even though we could not reach the classical 2.5D Sweet-Parker regime. In zero- β , reconnection is driven by the ideal self-pinching of quasi force-free thin current layers, whose subsequent diffusion leads to mass motion in the form of reconnection jets. This is exactly the same as in the case of separatrices. A feature that differs from reconnection in separatrices, however, is the development of fast slippage of magnetic field lines along QSLs during the whole process. We found that this slippage is the natural consequence of the local and gradual re-orientation of the magnetic field vector, as being due to local magnetic diffusion in the current layer, embedded in a continuum of field lines having sharp gradients of connectivity at the line-tied boundary. This allowed to put past analytical and numerical models of field line slippage (also referred to as field line flipping) in the frame of the single concept of QSLs.

We also reached the interesting conclusion that, when QSLs are thin enough (actually thinner than what is typically reached by large-scale shearing of initially low Q configurations in MHD simulations), the slippage velocities of the field

lines can be so fast that Alfvén waves traveling along them do not have the time to propagate from one footpoint to another. It follows that on MHD time scales, such slipping field lines can physically behave nearly as if they were reconnecting at separatrices, i.e. as if they instantaneously changed their connectivities. We call this new phenomenon *slip-running reconnection*. It fills the continuous gap between two extreme regimes: abrupt field line reconnection in separatrices (i.e. infinite slippage velocity) and very slow field line diffusion in braided flux tubes. During separatrix-less reconnection in 3D, we propose that a field line either *slips* or *slip-runs*, depending if its motion along the QSL is sub- or super-Alfvénic.

Aside from theoretical considerations, field line slippage offers a simple explanation for the puzzling motions of hard X-ray (HXR) sources, which move along chromospheric ribbons, as observed in some solar flares. In QSL reconnection, particles accelerated by super-Dreicer electric fields from a single coronal diffusion region within the QSLs, should quickly travel along field lines whose footpoint positions gradually move along the intersection of the QSL with the chromosphere, as slip-running reconnection proceeds. Theoretically, the speed and the extent of the HXR footpoint motions along the ribbons will depend not only upon the thickness of the QSL, but also on the relative position of the acceleration site with respect to the hyperbolic flux tube in the corona (which are not necessarily exactly co-spatial, as shown in Paper I) as well as on the relative values for all the time scales involved. These important issues will have to be addressed in a further study. Observationally, the finding of slip-running reconnection during solar flares, and its association with accelerated particles, requires the full tracing of fast-moving magnetic field lines, which can have an extended range of temperatures observable in EUV wavelengths, in conjunction with the moving locii of particle impacts in the chromosphere, visible in HXR. The unprecedented imaging qualities of the AIA instrument on the upcoming SDO, combined with RHESSI observations, will certainly be well suited for this study.

Appendix

The three columns of Figure 6 are available as GIF animations in the electronic version of Solar Physics. These animations show slip-running field lines with their footpoints being fixed in the $z = 0$ plane, during $0 \leq t - t^* \leq 28$ and using time-intervals of $dt = 2$. Supplementary material is available for this article at <http://dx.doi.org/10.1007/s11207-006-0230-2>.

Acknowledgements

The calculations in this paper were done on the Compaq-HP Quadri-Opteron computers of the Service Informatique de l'Observatoire de Paris (SIO). The authors

thank the referee for raising issues which helped to improve the quality of the paper. The work of C.R.D. was funded by NASA and ONR.

References

- Aly, J.-J.: 1990, in L. Dezső (ed.): *The Dynamic Sun*, Proc. 6th European Solar Phys. Meeting, *Publ. Debrecen Heliophys. Obs.* **7**, 176.
- Amari, T. and Luciani, J.-F.: 2000, *Phys. Rev. Lett.* **84**, 1196.
- Antiochos, S.K., Karpen, J.T., and DeVore, C.R.: 2002, *Astrophys. J.* **575**, 578.
- Aulanier, G., DeVore, C.R., and Antiochos, S.K.: 2006, *Astrophys. J.* **646**, 1349.
- Aulanier, G., Pariat, E., and Démoulin, P.: 2005, *Astron. Astrophys.* **444**, 961. (Paper I)
- Baty, H., Priest, E.R., and Forbes, T.G.: 2006, *Phys. Plasmas* **13**, 022312.
- Bhattacharjee, A., Ma, Z.W., and Wang, X.: 2003, *Lecture Notes in Physics* **614**, 351.
- Billinghamurst, M.N., Craig, I.J.D., and Sneyd, A.D.: 1993, *Astron. Astrophys.* **279**, 589.
- Bogachev, S.A., Somov, B.V., Kosugi, T., and Sakao, T.: 2005, *Astrophys. J.* **630**, 561.
- Büchner, J.: 2005, in Proceedings of the SPM11 Meeting, ESA SP-600, published on CDROM, p. 24.1.
- Büchner, J.: 2006, *Space Sci. Rev.* **122**, 149.
- Craig, I.J.D. and McClymont, A.N.: 1993, *Astrophys. J.* **405**, 207.
- Dauphin, C., Vilmer, N., and Anastasiadis, A.: 2006, *Astron. Astrophys.*, submitted for publication.
- Delannée, C. and Aulanier, G.: 1999, *Solar Phys.* **190**, 107.
- de Moortel, I. and Galsgaard, K.: 2006, *Astron. Astrophys.* **451**, 1101.
- Démoulin, P.: 2006, *Adv. Space Res.* **37**(7), 1269.
- Démoulin, P. and Priest, E.R.: 1997, *Solar Phys.* **175**, 123.
- Démoulin, P., Priest, E.R., and Lonie, D.P.: 1996, *J. Geophys. Res.* **101**, 7631.
- Démoulin, P., Hénoux, J.-C., Priest, E.R., and Mandrini, C.H.: 1996, *Astron. Astrophys.* **308**, 643.
- Démoulin, P., Bagalá, L.G., Mandrini, C.H., Hénoux, J.-C., and Rovira, M.G.: 1997, *Astron. Astrophys.* **325**, 305.
- DeVore, C.R., Antiochos, S.K., and Aulanier, G.: 2005, *Astrophys. J.* **629**, 1122.
- Fletcher, L. and Hudson, H.: 2002, *Solar Phys.* **210**, 307.
- Fletcher, L., López Fuentes, M.C., Mandrini, C.H., Schmieder, B., Démoulin, P., Mason, H.E. *et al.*: 2001, *Solar Phys.* **203**, 255.
- Forbes, T.G.: 1982, *J. Plasma Phys.* **27**, 491.
- Forbes, T.G. and Lin, J.: 2000, *J. Atmos. Solar-Terr. Phys.* **62**, 1499.
- Galsgaard, K.: 2000, *J. Geophys. Res.* **105**, 5119.
- Galsgaard, K., Titov, V.S., and Neukirch, T.: 2003, *Astrophys. J.* **595**, 506.
- Hesse, M. and Schindler, K.: 1988, *J. Geophys. Res.* **93**, 5559.
- Inverarity, G.W. and Titov, V.S.: 1997, *J. Geophys. Res.* **102**, 22285.
- Karpen, J.T., Antiochos, S.K., and DeVore, C.R.: 1991, *Astrophys. J.* **382**, 327.
- Karpen, J.T., Antiochos, S.K., DeVore, C.R., and Golub, L.: 1998, *Astrophys. J.* **495**, 491.
- Krucker, S., Hurford, G.J., and Lin, R.P.: 2003 *Astrophys. J.* **595**, L103.
- Lau, Y.T.: 1993, *Solar Phys.* **148**, 301.
- Longbottom, A., Rickard, G.J., Craig, I.J.D., and Sneyd, A.D.: 1998, *Astrophys. J.* **500**, 471.
- Longcope, D.W.: 2005, *Living Rev. Solar Phys.* **2**, 7 (cited on March 8, 2006).
- Longcope, D.W. and Magara, T.: 2004, *Astrophys. J.* **608**, 1106.
- Low, B.C. and Wolfson, R.: 1988, *Astrophys. J.* **324**, 574.
- Ma, Z.W. and Bhattacharjee, A.: 2001, *J. Geophys. Res.* **106**, 3773.
- Ma, Z.W., Ng, C.S., Wang, X., and Bhattacharjee, A.: 1995, *Phys. Plasmas* **2**, 3184.

- McClymont, A.N. and Craig, I.J.D.: 1996, *Astrophys. J.* **466**, 487.
- Petscheck, H.E.: 1964, in AAS-NASA Symposium on Solar Flares, NASA SP-50, p. 425.
- Poletto, G. and Kopp, R.A.: 1986, in D.F. Neiding (ed.), *The Lower Atmosphere of Solar Flares*, NSO/Sacramento Peak, Sunspot, p. 453.
- Pontin, D.I., Galsgaard, K., Hornig, G., and Priest, E.R.: 2005, *Phys. Plasmas* **12**, 052307.
- Priest, E.R. and Démoulin, P.: 1995, *J. Geophys. Res.* **100**, 23443.
- Priest, E.R. and Forbes, T.G.: 1992a, *J. Geophys. Res.* **97**, 16757.
- Priest, E.R. and Forbes, T.G.: 1992b, *J. Geophys. Res.* **97**, 1521.
- Priest, E.R. and Forbes, T.G.: 2000, *Magnetic Reconnection: MHD Theory and Applications*, Cambridge University Press, Cambridge.
- Priest, E.R., Heyvaerts, J., and Title, A.M.: 2002, *Astrophys. J.* **576**, 533.
- Priest, E.R., Hornig, G., and Pontin, D.I.: 2003, *J. Geophys. Res.* **108**, 1285.
- Priest, E.R., Longcope, D.W., and Heyvaerts, J.: 2005, *Astrophys. J.* **624**, 1057.
- Qiu, J., Jeongwoo, L., Gary, D., and Wang, H.: 2002, *Astrophys. J.* **565**, 1335.
- Strauss, H.R.: 1986, *Phys. Fluids* **29**, 3668.
- Sweet, P.A.: 1958, in IAU Symposium 6 on *Electromagnetic Phenomena in Cosmical Physics*, p. 123.
- Taylor, J.B.: 1974, *Phys. Rev. Lett.* **33**, 1139.
- Titov, V.S., Galsgaard, K., and Neukirch, T.: 2003, *Astrophys. J.* **582**, 1172.
- Titov, V.S., Hornig, G., and Démoulin, P.: 2002, *J. Geophys. Res.* **107**, SSH 3, 1.
- Titov, V.S., Priest, E.R., and Démoulin, P.: 1993, *Astron. Astrophys.* **276**, 564.
- Turkmani, R., Cargill, P.J., Galsgaard, K., Vlahos, L., and Isliker, H.: 2006, *Astron. Astrophys.* **449**, 749.
- van Tend, W. and Kuperus, M.: 1978, *Solar Phys.* **59**, 115.
- Wang, H., Yan, Y., Sakurai, T., and Zhang, M.: 2000, *Solar Phys.* **197**, 263.
- Yokoyama, T. and Shibata, K.: 1994, *Astrophys. J.* **436**, L197.